Proceedings of the 11th Brazilian Congress of Thermal Sciences and Engineering – ENCIT 2006
Braz. Soc. of Mechanical Sciences and Engineering – ABCM, Curitiba, Brazil, Dec. 5-8, 2006

Paper CIT06-0721

Numerical computation of the flow around rough elements

Daniel A. Rodrigues
Programa de Engenharia Mecânica,
Universidade Federal do Rio de Janeiro, C.P. 68503, 21945-970, Rio de Janeiro
darodrigues@mecanica.coppe.ufrj.br

Alexandre T. P. Alho
Programa de Engenharia Naval e Oceânica,
Universidade Federal do Rio de Janeiro, C.P. 68503, 21945-970, Rio de Janeiro
alho@peno.coppe.ufrj.br

Atila P. Silva Freire
Programa de Engenharia Mecânica,
Universidade Federal do Rio de Janeiro, C.P. 68503, 21945-970, Rio de Janeiro
atila@mecanica.coppe.ufrj.br

Abstract. *The present work shows how numerical computations on the flow around a rough element can be used to find reliable results for the wall shear stress and the displacement in origin for the flow over a fully rough surface. The numerical computations are combined with the integral methods of Perry and Joubert (1963, JFM, 17, 193:211) and of Perry et al. (1969, JFM, 37, 383:413) to find reliable data for the error in origin that can be used to explain how the shear stress develops. All procedures are tested against hot-wire data obtained in a low turbulence wind-tunnel. In fact, four different methods are used to find the shear stress at the wall: the classical momentum integral equation, the velocity gradient method of Perry and Joubert (1963), the Reynolds shear stress in the surface layer and a momentum balance around a single rough element.*

keywords: *Roughness, CFD, BSL-RSM, wall shear stress, error in origin.*

1. Introduction

The description of turbulent flow over a rough surface is a central problem in fluid mechanics. Since most surfaces in nature and in technology are rough, the interest arose by this subject is indeed very high. Unfortunately, the physical and mathematical modeling of such flow is inherently difficult. The following statement by Schlichting makes this clear: "The desire to explore the laws of friction of rough pipes in a systematic way is frustated by the fundamental difficulty that the number of parameters describing roughness is extraordinarily large owing to the great diversity of geometric forms" (H. Schlichting, Boundary Layer Theory, 7th edition, page 615).

Despite the aforementioned difficulty, the advances were many. As early as 1923, Hopf identified two types of roughness. If surfaces were formed by relatively coarse and tightly spaced elements (sand grains, cast iron, cement), flow resistance was observed to be proportional to the square of velocity (Reynolds number independence). In this case, the effects of roughness could be expressed with the aid of a single roughness parameter. If, however, surfaces were formed by gentle protusions distributed over a relatively large area, flow resistance depended both on Reynolds number and on a roughness parameter. A few years later, Einstein and El-Samni (1949) observed that for flow over a rough surface the velocity profiles should be plotted considering that a theoretical wall was set at distance below the top of the rough elements. The concept of a displacement in origin was further studied by Perry and Joubert (1963). These same authors in a sequence paper (Perry et al., 1969) identified two wall geometries that resulted in different log-law behaviors: one type with a reference length based on the size of the roughness (termed a 'k'-type roughness), the other type with a reference length based on the pipe diameter (termed a 'd'-type roughness).

A major difficulty in developing models for flows over rough surfaces is to measure the wall shear stress. All traditional methods developed for smooth walls including the Preston or Stanton tubes, momentum integral methods and the gradient graphical method are highly inaccurate. As an alternative, more reliable method, Perry et al. (1969) proposed to find the wall shear stress by pressure tapping the roughness elements and assessing their form drag.

The objective of the present work is to assess the current state of turbulence models in regard to the numerical simulation of flows over a rough surface. In particular, one turbulence model will be considered: the Baseline Reynolds Stress Model (BSL-RSM). This model does not use the eddy viscosity hypothesis but solves a system of transport equations for all components of the Reynolds stress tensor. The possibility of inherently accounting for stress anisotropies makes the BSL-RSM a good choice for the description of complex flows.

A common practice in the numerical simulation of turbulent flows is to consider the existence of a near wall region where local solutions can actually be used to provide wall boundary conditions. For rough walls, a local logarithmic profile can be specified in terms of a roughness reference length, the so-called 'equivalent sand grain roughness' (Nikuradse (1932)). This length, unfortunately, is not exactly equal to the real roughness height; it also depends on other properties of the wall including shape, distribution, etc. This single feature makes the use of log-laws very uncertain for flow over rough surfaces.

Here, the solution strategy will be different. Instead of using log-laws to specify the wall boundary conditions we will follow the following procedure. First, the flow domain is discretized and solved considering every roughness element individually. Having obtained local solutions for the mean and fluctuating quantities, four different methods are then used to post-process the numerical data and find the wall shear stress. These four methods are based on i) the momentum integral equation, ii) the form drag of the individual roughness elements, iii) the spatial average of the Reynolds shear stress and iv) the velocity gradient method of Clauser (1954). With the resulting reliable data that is obtained for the wall shear stress, the logarithmic profile can then be re-constructed to find the reference roughness length of the surface and the displacement in origin. These are the two parameters of engineering relevance.

The present calculation procedure is then compared with some new experimental data. With tunnel experiments over a rib-type surface are carried out to provide data of local mean and turbulent quantities.

2. Determination of wall shear stress

One of the simplest ways to find the wall shear stress is to consider the momentum integral equation, which can be cast as

$$\frac{c_f}{2} = \frac{\theta}{U_1}(2+H)\frac{dU_1}{dx} + \frac{d\theta}{dx} \tag{1}$$

where, U_1 denotes the external flow velocity, δ^* is the displacement thickness, θ is the momentum thickness and $H{=}\delta^*/\theta$ is the shape factor.

Although very useful, Eq. 1 has the disadvantage of relying on a differentiation to find c_f. The consequence is that a large sampling of θ must be considered and any necessary curve fitting must be carefully considered.

The evaluation of c_f by pressure tapping individual roughness elements was described in Perry et al. (1969). By drawing a control volume with a unit lateral length around a single element, a simple balance of the x-momentum results in

$$c_f = \frac{\tau_0}{(1/2)\rho U_0^2} = \frac{k}{\lambda}(C_{D0} - \frac{\Delta P_L}{(1/2)\rho U_0^2}) \tag{2}$$

where, τ_0 is the effective shear stress acting over the wall, k is the roughness height, λ is the roughness pitch, ΔP_L is the external pressure gradient, U_0 is the external flow velocity and

$$C_{D0} = \frac{1}{k(1/2)\rho U_0^2}\int_0^k (P_2(y) - P_3(y))dy \tag{3}$$

with $P_2(y)$ and $P_3(y)$ the pressures measured on the surface of the individual roughness elements as a function of the distance from the wall.

The term C_{D0} can can also be evaluated from an integral momentum balance of the outer flow on the control volume defined in Perry et al. (1969), according to

$$C_{D0} = -\frac{2\Delta\theta}{\Delta x} = \frac{1}{(1/2)U_0^2}(\frac{1}{\lambda}\int_x^{x+\lambda}\overline{(u'v')}dx + \frac{1}{\lambda}\int_x^{x+\lambda}(u_0 v_0)dx) \tag{4}$$

where $\overline{(u'v')}$ denotes the turbulent shear stress and $(u_0 v_0)$ the product of the temporal mean horizontal and vertical velocity components along the top of the control volume.

The local wall shear stress can also be determined by plotting the mean velocity profile on coordinates $\overline{U}$ against y. This procedure is known as the Clauser chart method. For a rough surface, Einstein and El-Samni (1949) showed that the origin of the y-axis must be taken some distance below the top of the roughness elements. This distance, hereafter denoted by ε, defines a coordinate system that will give a logarithmic distribution of velocity near the wall.

Hence, the mean velocity profile is to be written as

$$\frac{u}{u_\tau} = \frac{1}{\varkappa} \ln\left(\frac{(y_T + \varepsilon)u_\tau}{\nu}\right) + A + -\frac{\Delta u}{u_\tau} + W(y/\delta) \tag{5}$$

where u_τ is the friction velocity, $\varkappa$ is von Karman's constant (=0.4), y_T is the distance taken from the top of the roughness elements, A is the classical constant in the law of the wall (=5), Δu is Nikuradse's roughness function, and W Coles' wake function.

On a log-graph, the above equation appears as a straight line so that its slope and position can be used to determine u_τ. Unfortunately, a large number of possible combinations of parameters u_τ, Δu, and ε will give straight lines with a good coefficient of correlation. In this sense, Eq. 5 is of limited use for the determination of u_τ. However, provided u_τ is known, Eq. 5 can be used to find ε and Δu.

The error in origin was shown by Jackson (1981) to correspond to the average displacement height of the total shear stress (defined by Eq. 6 below). In fact, if we make $d = k$ - ε, that is, if we take as the reference surface the bottom of the rough elements, then it is possible to write

$$d - \overline{h} = \frac{1}{\lambda \tau_0} \int_{fluido} (\tau_0 - (T_{12} - \rho uv))\, dxdy \tag{6}$$

with $\overline{h} = (kl/\lambda)$, l = width of rough elements,

$$T_{12} = -\rho\overline{u'v'} + \mu\frac{\partial u}{\partial y}, \tag{7}$$

$$\tau_0 = [T_{12} - \rho\overline{uv}]_{y=\delta_i}, \qquad \delta_i = \text{height of control volume} \tag{8}$$

3. Turbulence models

The numerical simulations will be performed with a Reynolds Stress-ω model, the baseline (BSL-RSM) Reynolds Stress turbulence model. This selection of models is considered representative enough of the state of the art in turbulence engineering modeling to allow for a good assessment of the numerical computations of the flow over a rough surface. The advantage of ω-equation based models is that they have a more accurate near wall treatment.

The equations of motion are the Reynolds averaged equations of continuity and momentum for an incompressible flow. Denoting the mean and fluctuating velocities in x_i-direction by U_i and u_i respectively, the density and kinematic viscosity by ρ and ν and mean pressure by P, the equations can be written as

$$\partial_i U_i = 0, \qquad \partial_t U_i + U_j\, \partial_j U_i = -\partial_i P + \partial_j[\nu(\partial_j U_i + \partial_i U_j) - \overline{u_i u_j}] \tag{9}$$

where Einstein's notation of repeated indexes has been used for conciseness.

The pressure term has been divided by density.

A general way to model a turbulent flow is to compute every component of the Reynolds stress tensor from transport equations derived directly by algebraic manipulations of the Navier-Stokes equations. The resulting loss of information implied by the averaging process must then be recovered by an adequate modeling of each of the terms present in the equations. Most models consider the same basic set of rules to close the equations. All turbulent quantities are considered to be a function of Reynolds stress, κ, ϵ (or alternatively ω), mean flow quantities and related thermodynamics variables. The diffusion of turbulent quantities, in particular, is taken

to be proportional to the local gradient of the quantity. The dissipation of turbulent kinetic energy is supposed to occur at very small scales where turbulence is isotropic.

Constants appearing in the models are *ad hoc* so that they must be fixed through experimental calibration. The models also need to be consistent with the common requirements of symmetry, invariance and permutation.

Models that use the ϵ-equation frequently have to resort to complex non-linear damping functions in the near wall region. An alternative two-equation model that is claimed to circumvent this difficulty is the κ-ω model (Wilcox (1988)). In fact, the great advantage of the κ-ω formulation is supposed to be exactly the near-wall treatment, which can accept higher values of y^+=(yu_τ/ν), the non-dimensional distance from the wall. The κ-ω model has the additional advantage of providing near wall analytical solutions for both the viscous and the fully turbulent regions.

Despite the superior handling of the wall conditions, the κ-ω formulation struggles with its strong sensitivity to free stream conditions. Thus, given the different zonal strengths and, for that matter, weaknesses of the κ-ϵ and the κ-ω formulations, a good balance can be achieved between both models if a blending is introduced between the κ-ω formulation near the surface and the κ-ϵ model in the outer flow. This solution was proposed by Menter (1994), who introduced the so-called baseline κ-ω model (BSL).

The Reynolds stress model, formulated in terms of the ω-equation, can be written as

$$\partial_t(\overline{u_i u_j}) + \partial_k(U_k \overline{u_i u_j}) = \partial_k\Big(\Big((\nu_t/\sigma^*) + \nu\Big)\partial_k \overline{u_i u_j}\Big) - P_{ij} - \Pi_{ij} + (2/3)\beta'\omega\kappa\delta_{ij} \tag{10}$$

The ω-equation, can be written as

$$\partial_t\omega + \partial_k U_k\omega = \partial_k\Big(\Big(\nu + \nu_t/\sigma_{\omega 3}\Big)\partial_k\omega\Big) - \alpha_3\frac{\omega}{\kappa}P - \beta_3\omega^2 + 2(1-F_1)(\sigma_2\omega)^{-1}\partial_k\kappa\partial_k\omega. \tag{11}$$

The coefficients in the ω-equation (with subscripts 3) are blended between two sets of constants, one to be used near the wall corresponding to ω-based models (with subscripts 1, given below, Eqs. 19) and another used in the free stream corresponding to ϵ-based models (with subscripts 2, given below, Eqs. 20).

The definition of the several terms in the above equations is

$$\nu_t = \kappa/\omega, \tag{12}$$

$$P_{ij} = \tau_{ik}\partial_k U_j + \tau_{jk}\partial_k U_j,\ \tau_{ik} = -\overline{u_i u_k}; \qquad P = (1/2)P_{kk} \tag{13}$$

$$D_{ij} = \tau_{ik}\partial_j U_k + \tau_{jk}\partial_i U_k, \tag{14}$$

$$\Pi_{ij} = \beta' C_1\omega\,(\tau_{ij} + (2/3)\kappa\delta_{ij}) - \hat{\alpha}\,(P_{ij} - (2/3)P\delta_{ij}) - \hat{\beta}\,(D_{ij} - (2/3)P\delta_{ij}) - \hat{\gamma}\kappa\,(S_{ij} - (1/3)S_{kk}\delta_{ij}) \tag{15}$$

The blending of coefficients is made through the following linear interpolation function

$$\phi_3 = F\phi_1 + (1-F)\phi_2, \qquad \phi = \text{dummy variable} \tag{16}$$

where $F = \tanh(\arg^4)$ with

$$\arg = \min\Big[\max\Big(\frac{\sqrt{\kappa}}{\beta'\omega\,y}, \frac{500\nu}{y^2\omega}\Big), \frac{4\rho\kappa}{CD_{\kappa\omega}\ \sigma' y^2}\Big] \tag{17}$$

and

Figure 1: General view of wind tunnel.

$$CD_{\kappa\omega} = \max\Big(2\rho(\sigma'/\omega)\nabla\kappa\nabla\omega, 10^{-10}\Big), \qquad \sigma' = 1/0.856 \tag{18}$$

where the following model constants apply

$$\omega - \text{region},\ \sigma_1^* = 2,\ \sigma_1 = 2,\ \beta_1 = 0.075,\ \alpha_1 = 0.553 \tag{19}$$

$$\epsilon - \text{region},\ \sigma_2^* = 1,\ \sigma_1 = 0.856,\ \beta_2 = 0.0828,\ \alpha_2 = 0.44 \tag{20}$$

and

$$\sigma^* = 2,\ \sigma' = 1.168,\ \beta' = 0.09,\ \hat{\alpha} = 0.775,\ \hat{\beta} = 0.196,\ \hat{\gamma} = 0.495. \tag{21}$$

4. Experimental procedure

The experiments were carried out in the low-turbulence wind tunnel located in the Laboratory of Turbulence Mechanics of PEM/COPPE/UFRJ. The tunnel is an open circuit tunnel with a test section of dimensions 300 mm x 300 mm x 4,000 mm. The test section is divided into two sections of equal length which can be fitted with surfaces having different types of roughness. In the present experiment however, just one type of rough surface was tested. A general view of the wind tunnel is shown in Fig. 1.

The rough surface was a rib-type roughness constructed with rectangular aluminum bars of 6.35 by 4.76 mm rectangular cross section (see Fig. 2). The flow before reaching the rough surface traveled through a short smooth surface section whose leading edge was faired into the wind-tunnel floor by a 200-mm long ramp.

Every roughness element was made removable so that another element constructed with pressure taps could be fitted anywhere in the roughness pattern. The pressure taps, seven in all, were drilled directly onto an aluminum bar. The pressure tubes were connected directly to an inclined manometer that was operated at an angle of 2^o and was filled with alcohol. Pressures were therefore measured to an accuracy of 0.028 mm of water.

Instrumentation consisted of hot-wire anemometry. The x-probes, Dantec model P61, were operated by two Kauri constant temperature bridges. Probes were calibrated against a Pitot-static tube at the beginning of each run. The data was acquired at with a sampling frequency of 10.000 Hz and sampling time of 50 s. An uncertainty analysis of the data was performed according to the procedure described in Kline (1985). The uncertainty associated with the velocity measurements was: $U = 0.064$ m/s precision, 0 bias (P=0.95).

To obtain accurate measurements (Bruun (1985)), the mean and fluctuating components of the output signal of the anemometer were treated separately. Two output channels of the anemometer were used. The mean velocity profiles were calculated directly from the untreated signal of channel one. The signal given by channel two was 1 Hz high-pass filtered leaving, therefore, only the fluctuating velocity. The later signal was then amplified with a gain controlled between 1 and 500 and shifted by an offset so as to adjust the amplitude of the signal to the range of the A/N converter.

The measurements were performed for values of the free-stream velocity of 8 m/s; the free stream-level of turbulence was about 0.2%. .

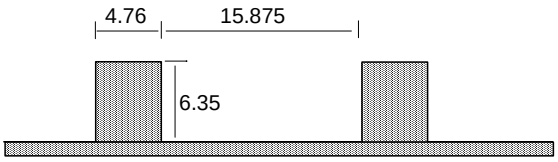

Figure 2: Geometry of roughness elements. Dimensions are in mm.

Figure 3: Detail of ramp and of pressure taps.

5. Computational details

The equations governing the problem were solved using the well known code ANSYS CFX, release 10. The model solves the Reynolds averaged Navier-Stokes equations (RANS) through a finite-volume approach. The solution strategy consists in solving the momentum equations using a guessed pressure. Next, a pressure correction is obtained which typically needs a large number of iterations to reach a converged solution. The code uses a coupled solver that solves the equations for the flow parameters as a single system. This procedure uses a fully implicit discretization of the equations at any given time. In the present steady state case, the time step behaves like an acceleration parameter to find the approximate solutions in a physically meaningful framework to a time independent solution.

The dimensions of the computational domain were defined in accordance to the experimental model. However, due to the high computer-storage and runtime efforts that are necessary to carry out computations over the full length of the experimental model, the extension of the computational domain was defined so as to include just two consecutive measurement stations. That meant performing the computations over five roughness elements. This strategy permitted the specification a very refined grid, particularly around the roughness elements where high velocity gradients occur. The height of the computational grid was taken to be twice the local boundary layer thickness to keep to a minimum any boundary condition influence on computations for the surface layer. A two-dimensional model was achieved by considering just one grid element in w-direction.

The above solution strategy depends for its success on a very fine representation of the near wall region. The present version of ANSYS CFX 10.0, controls near wall computations by an automatic method. Depending on the mesh refinement in the near-wall region, the method automatically switches the solution approach from wall-functions to a low-Re near wall formulation. The controlling parameter is the viscous region scale y^+ ($=y\ u_\tau/\nu$). Provided $y^+ < 2$, the low-Re model will be employed. With the present mesh, y^+ varies between 1.96 and 0.62.

Computations were carried out on a series of structured meshes that were generated consisting of hexahedrons. An extensive grid-dependence test was performed resulting in a final non-uniform, body-fitted mesh with 486.102 elements. The mesh was particularly refined in the near wall region so as to completely resolve the inner turbulent and viscous sub-layers. The refined mesh region extended up to 1.0 k (k = roughness height) above the top of the roughness elements.

Inlet conditions were prescribed directly from the experimental data. At the outlet, the turbulent intensity was automatically calculated by the model. At the side walls a symmetry condition was imposed. At ground level, the no-slip boundary condition was used.

The computations were performed on two Pentium 4, 3.0 GHz, with 2 Gb DDR400 RAM operating in a cluster configuration.

6. Results

Comparison will be made for the second measuring station. The general flow pattern that is formed in the cavity defined by two consecutive roughness elements is shown in Fig. 4 as yielded by the BSL-RSM model. A large recirculating flow region is observed which, however, does not span the whole length of the cavity. In fact, two large regions of recirculating flow are identified. In a 'd' type rough wall, stable vortices are formed in the cavities and shedding from the protuberances into the flow is negligible. In this case, the external flow passes relatively undisturbed over the top of the protuberances. In a 'k' type rough wall, on the other hand, large eddies with a length scale proportional to the height of the roughness elements are shed into the external flow blending smoothly with the surroundings. According to the present computations, our present roughness appears to be of the 'd' type. In fact, it must be pointed out that the present flow pattern is somewhat different from the flow visualization studies that were presented in Perry et al. (1969). In this work, for both 'd' and 'k' type roughness, just one large eddy was observed to develop in the cavities. Here, however, two large eddies are apparent. A distinct feature of a 'd' type roughness, however, is the presence of a stagnation streamline on the leading face of the roughness element. Notice the pressure distribution on both sides of the roughness elements (Fig. 5). A stagnation streamline is located very close, but below, to the top of the protuberances.

Figure 5) presents data for the numerical pressure distribution prediction, as well as data obtained directly from the pressure readings. With the help of Eq. 2, the skin-friction velocity can be evaluated from a direct numerical integration of the pressure profiles given by both procedures.

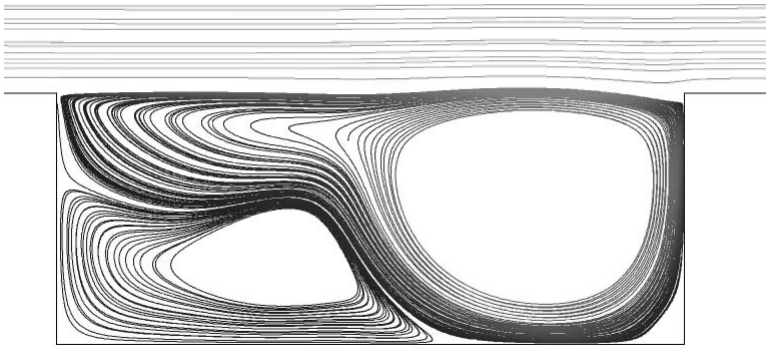

Figure 4: Flow streamlines between roughness elements.

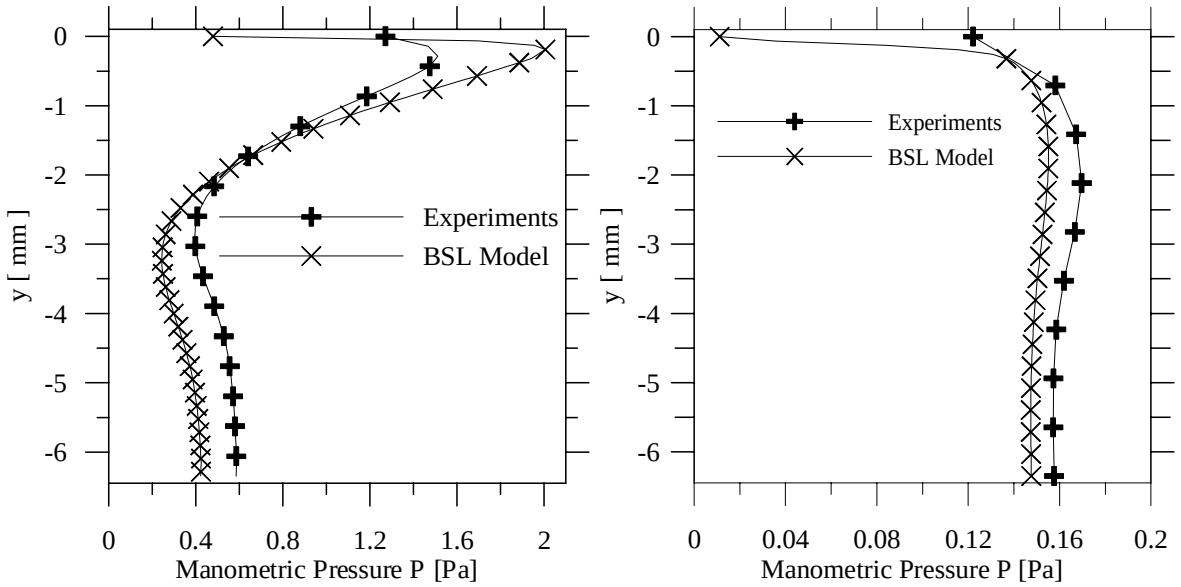

Figure 5: Pressure distribution around roughness elements.

Over a rough surface, the flow structure has to contain at least two characteristic regions. Adjacent to the rough wall the flow is strongly influenced by each roughness element and is not spatially homogeneous. This region, the roughness sublayer (RS), has a thickness of about 2-5k. Above the RS there is an inertial sublayer (IS) within which similarity theory is applicable. Therefore, in the IS the flow properties are homogeneous on the scale of the roughness spacing, the mean velocity profile is logarithmic and the turbulent statistics are nearly constant.

The velocity distribution in different flow stations is shown in Fig. 6a in linear coordinates. The extent of the inertial sublayer can be seen in Fig. 6b where the profiles are plotted in semi-log co-ordinates. Predicted turbulence properties are seen in Fig. 7. The longitudinal Reynolds stresses are underestimated by the BSL-RSM model by almost one third of its experimental value in the near wall region. The shear stresses are also much underestimated, now by a margin of 50% of the experimental values.

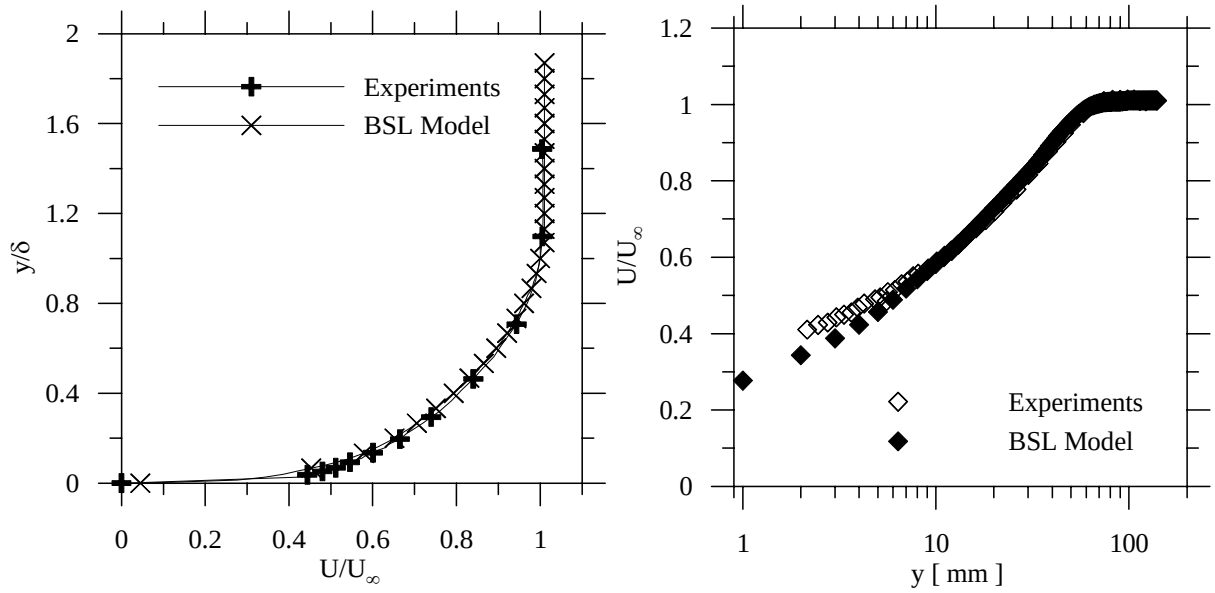

Figure 6: Velocity distribution on top of roughness elements.

The shear stress in the inertial region is often used by authors to evaluate the surface shear stress. By averaging $u'v'$ in the inertial region one may consider $\sqrt{-\overline{u'v'}} = u_\tau$. However, within the RS, $u'v'$ varies significantly with both y and x (Cheng and Castro, 2002). The implication is that the height where the averaging of $u'v'$ is to be taken must be chosen judiciously. Figure 8 shows the predicted values of $\overline{-u'v'}$ according to the BSL-RSM for various distances above the roughness element. For very short distances from the wall, the shear stress is observed to oscillate strongly. For the highest distance, $y/k = 1.0$, the shear stress is observed to drop to some very low values, much below the significant values near the wall.

The prediction of u_τ according to the several techniques introduced in this work is presented in Fig. 9. The overall agreement is very good.

7. Final Remarks

The present word has shown how sophisticated computational techniques can be combined with classical procedures to furnish reliable data on the wall shear stress for flows over rough surfaces. The proposal here was to use CFD to find local results that upon a further processing through integral methods resulted in reliable wall shear stress predictions.

Overall, the mean results were very good. However, prediction of turbulent quantities was very poor. In fact, due to the complexity of the problem this was the expected trend. The proposed method to find u_τ was then conceived to be robust and dependent on mean flow properties. The feature makes this method a very attractive method to be used in the determination of the displacement in origin and of the effective roughness.

Acknowledgements. APSF is grateful to the Brazilian National Research Council (CNPq) for the award of a Research Fellowship (Grant No 304919/2003-9). The work was financially supported by CNPq through Grant No 472215/2003-5 and by the Rio de Janeiro Research Foundation (FAPERJ) through Grants E-26/171.198/2003 and E-26/152.368/2002.

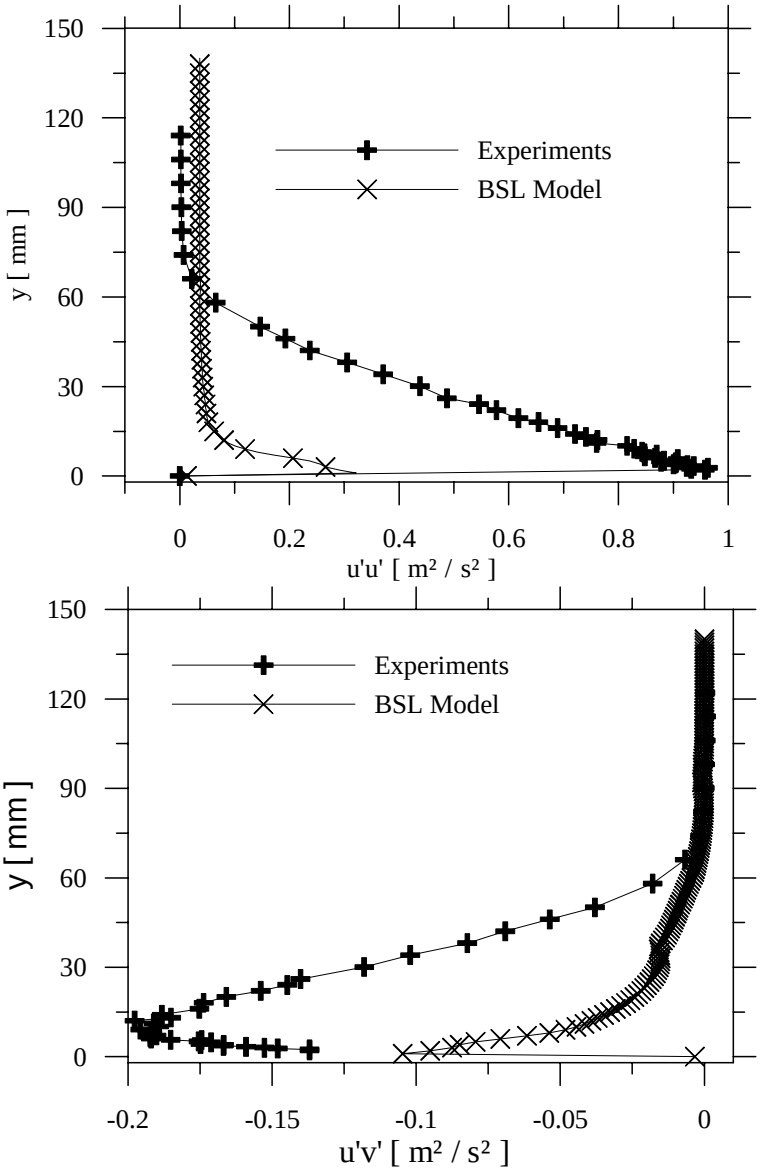

Figure 7: Turbulent longitudinal and shear stresses on top of roughness elements.

8. References list

Bruun, H. H., 1995, Hot-wire Anemometry - Principles and Signal Analysis, Oxford University Press.

Cheng, H. and Castro, I. P., 2002, Near-Wall Flow Development After a Step Change in Surface Roughness, BLM, 105, 411-432.

Einstein, H.A., El-Samni, E.-S. A., 1949, Hydrodynamic forces on a rough wall, Review of Modern Physics, 21, 520–524.

Hopf, L. 1923, Die Messung der Hydraulischen Rauhigkeit, ZAMM, 3, 329-339.

Kline, S.J., 1985, The Purpose of Uncertainty Analysis, J. Fluids Engineering, 107, 153-160.

Nikuradse, J., 1933, Stromungsgesetze in Rauhen Rohren, Forschg. Arb. Ing.-Wes. No 361.

Perry, A.E., and Joubert, P.N., 1963, Rough Wall Boundary Layers in Adverse Pressure Gradients, J. Fluid Mechanics, 17, 193–211.

Perry, A.E., Schofield, W.H. and Joubert, P.N., 1969, Rough Wall Turbulent Boundary Layers, J. Fluid Mechanics, 37, 383–413.

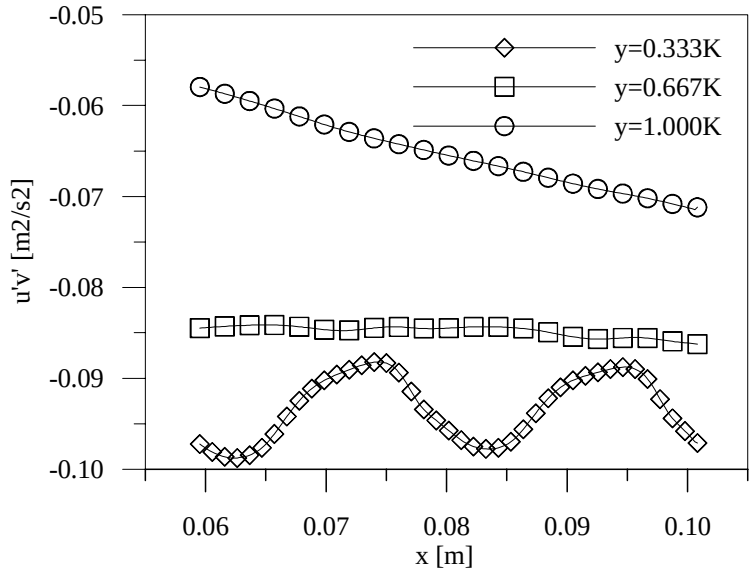

Figure 8: Predictions of $\overline{-u'v'}$ according to the BSL-RSM.

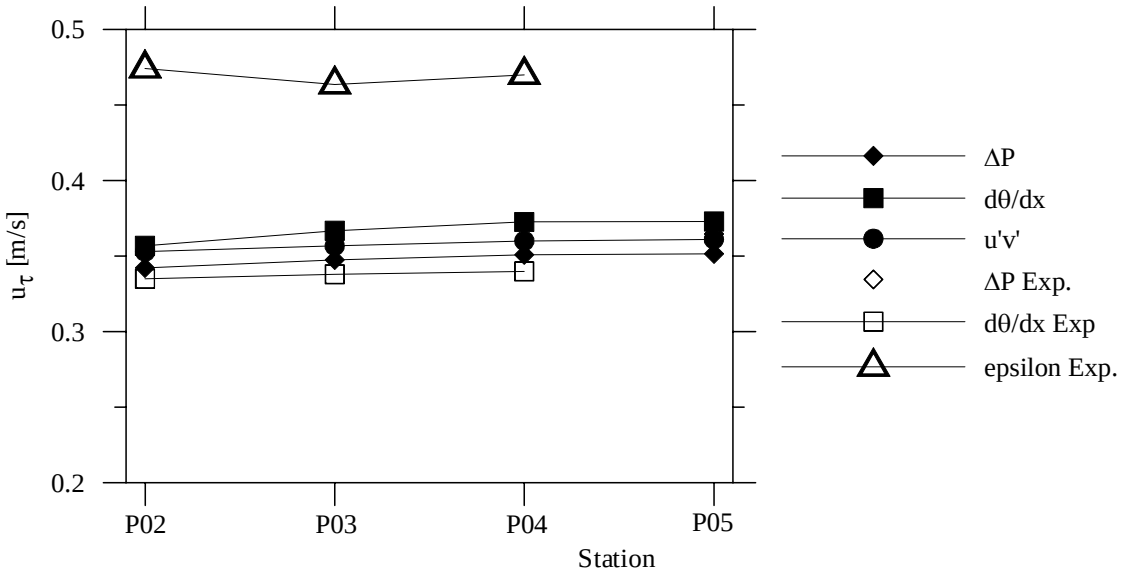

Figure 9: Predictions of u_τ according to the several techniques compared with the experimental data.